ROTATING DISK FLOW STABILITY IN ELECTROCHEMICAL CELLS

J. Pontes
Metallurgy and Materials Engineering Department – EE/COPPE/UFRJ
PO Box 68505, 21945-970 Rio de Janeiro RJ, Brazil
jopontes@.ufrj.br

Norberto Mangiavacchi
Institute of Mathematical and Computational Sciences USP – S. Carlos,
PO Box 668, 13560-161 S.Carlos, SP, Brazil
norberto@icmc.sc.usp.br

Anderson R. Conceição
Metallurgy and Materials Engineering Department – EE/UFRJ
PO Box 68505, 21945-970 Rio de Janeiro RJ, Brazil
anderson@metalmat.ufrj.br

Oswaldo E. Barcia
Institute of Chemistry – UFRJ,
PO Box 68505, 21945-970 Rio de Janeiro, Brazil
barcia@metalmat.ufrj.br

Oscar Rosa Mattos
Metallurgy and Materials Engineering Department – COPPE/UFRJ
PO Box 68505, 21945-970 Rio de Janeiro RJ, Brazil
omattos@metalmat.ufrj.br

Bernard Tribollet
UPR15 – CNRS, Physique des Liquides et Electrochimie,
4 place Jussieu, 75252 Paris Cedex 05, France
bt@ccr.jussieu.fr

Abstract. *P*olarization curves experimentally obtained in the electro-dissolution of iron in a 1 **M H_2SO_4** solution using a rotating disk as the working electrode present a current instability region within the range of applied voltage in which the current is controlled by mass transport in the electrolyte. According to the literature (Barcia *et. al*, 1992) the electro-dissolution process leads to the existence of a viscosity gradient in the interface metal-solution. The viscosity gradient changes the velocity field and may affect the stability properties of the steady flow developed close to the rotating disk electrode. On a previous paper, Pontes *et. al* (2002) showed that this is indeed the case when the steady flow is perturbed by disturbances with periodic variation along the radial direction. In this paper we extend those results by considering the linear stability of the flow with respect to perturbations with periodic variation along the radial and azimuthal directions. It is shown that the neutral stability curves are modified by the presence of a viscosity gradient and the critical Reynolds number beyond which perturbations are amplified is reduced in most cases. The neutral curves for perturbations turning with several angular velocities are presented and the results are compared with those presented by Malik (1986) and Lingwood (1995). Results for constant viscosity fluids show good agreement with those existing in the literature and are used to validate the numerical code developed to perform the linear stability analysis of the steady flow. The results presented support the hypothesis that the current oscillations observed in the polarization curve may originate from a hydrodynamic instability.

Keywords:*Rotating Disk Flow, Electrochemical Instabilities, Hydrodynamic Stability, Turbulence*

1. Introduction

Polarization curves experimentally obtained in the electro-dissolution of iron in a 1 **M H_2SO_4** solution using a rotating disk as the working electrode present three different regions (Barcia *et. al*, 1992). The first region is associated with low over-voltages applied to the working electrode and the current is a function of the electric potential and dissolution process only. The electric current is controlled by the transfer of charges at the interface rotating disk/electrolyte solution, and the mass transport does not affect the electro-dissolution process. By increasing the the applied potential, the curves show a second region where the hydrodynamic conditions, which depend on the angular velocity imposed to the rotating disk electrode, affect the rate of the anodic dissolution of iron. The current is a function both of the applied potential and the hydrodynamic field developed close to the rotating electrode. By further increasing the applied over-voltage a third region appears, where the current is totally controlled by mass-transport processes.

In this third region, polarization curves present a current plateau, defining a limit value for the current, which depends on the hydrodynamic conditions set by the angular velocity of the electrode.

Two current instabilities are observed in the third region: one at the beginning of the current plateau and a second one at the end, where the electrode surface undergoes an active to passive transition (Ferreira *et. al*, 1994). The first instability is intrinsic to the system, while the current instability close to the active-passive transition is affected by the output impedance of the control equipment. This instability can be suppressed by using a negative feedback resistance (Epelboin, 1972), that gives rise to a continuous curves. Barcia et. al. (1992) proposed that the electro-dissolution process leads to the existence of a viscosity gradient in the diffusion boundary layer, which modifies the steady velocity field close to the electrode and could affect the stability of the hydrodynamic field. On a previous paper, Pontes *et. al* (2002) showed that this is indeed the case when the steady rotating disk flow is perturbed by disturbances with periodic variation along the radial direction. The base state was assumed as the classical rotating disk flow (Von Kármán, 1921 Schlichting, 1968), modified by the existence of a viscosity gradient pointing along the axial direction. In this paper we extend those results by considering the stability of the flow with respect to perturbations with periodic variation along the radial and azimuthal directions. The results are compared with those presented by Malik (1996), Faller (1991) and Lingwood (1996).

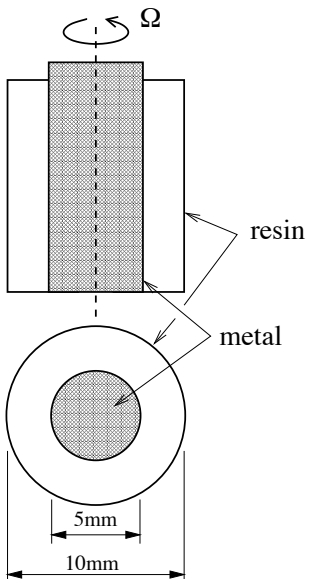

Fig. 1: The rotating disk electrode

For a review of the literature concerning current instabilities in electrochemical cells and in rotating disk flow of fluids with constant viscosity, the reader is referred to the paper by Pontes *et. al* (2002).

The paper is organized as follows: Section (2) describes the steady velocity flow, which is the problem base state, for the case of constant viscosity fluids and for six viscosity profiles configurations assumed in this work. Section (3) deals with the linearized equations of the perturbed flow. Section (4) presents the neutral curves obtained by spanning the parameter space of the problem and solving the eigenvalue/eigenfunction problem for constant and variable viscosity fluids. Conclusions are presented in Sec. (5).

2. The Base State

The steady hydrodynamic field is the well known Von Kármán (1921) exact solution of the continuity and Navier-Stokes equations for laminar rotating disk-flow, written in a rotating coordinate frame turning with the disk angular velocity Ω:

$$\mathbf{div}\,\mathbf{v} = 0 \tag{1}$$

$$\frac{D\mathbf{v}}{Dt} = -2\Omega \times \mathbf{v} - \frac{1}{\rho}\,\mathbf{grad}\,p + \frac{1}{\rho}\,\mathbf{div}\,\tau \tag{2}$$

where $-2\Omega \times \mathbf{v} = 2\Omega\,(v_\theta \mathbf{e}_r - v_r \mathbf{e}_\theta)$ and τ is the viscous stress tensor for a Newtonian fluid with the viscosity μ depending on the axial coordinate z. The components of stress tensor are given by (Schlichting, 1968):

$$\left.\begin{aligned} \tau_{rr} &= 2\mu\frac{\partial v_r}{\partial r} & \tau_{r\theta} &= \tau_{\theta r} = \mu\left(r\frac{\partial}{\partial r}\left(\frac{v_\theta}{r}\right) + \frac{1}{r}\frac{\partial v_r}{\partial \theta}\right) \\ \tau_{\theta\theta} &= 2\mu\left(\frac{1}{r}\frac{\partial v_\theta}{\partial \theta} + \frac{v_r}{r}\right) & \tau_{\theta z} &= \tau_{z\theta} = \mu\left(\frac{\partial v_\theta}{\partial z} + \frac{1}{r}\frac{\partial v_z}{\partial \theta}\right) \\ \tau_{zz} &= 2\mu\frac{\partial v_z}{\partial z} & \tau_{rz} &= \tau_{zr} = \mu\left(\frac{\partial v_r}{\partial z} + \frac{\partial v_z}{\partial r}\right) \end{aligned}\right\} \tag{3}$$

The steady solution takes the form:

$$\bar{v}_r = r\,\Omega\,F(\xi) \tag{4}$$

$$\bar{v}_\theta = r\,\Omega\,G(\xi) \tag{5}$$

$$\bar{v}_z = (\nu(\infty)\,\Omega)^{1/2}\,H(\xi) \tag{6}$$

$$\bar{p} = \rho\nu(\infty)\Omega P(\xi) \tag{7}$$

where $\xi = z(\Omega/\nu(\infty))^{1/2}$ and $\nu(\infty)$ is the bulk viscosity, far from the electrode surface. Equations (4–7) are introduced in the dimensional continuity and Navier-Stokes equations, leading to the following system of equations for F, G, H and P.

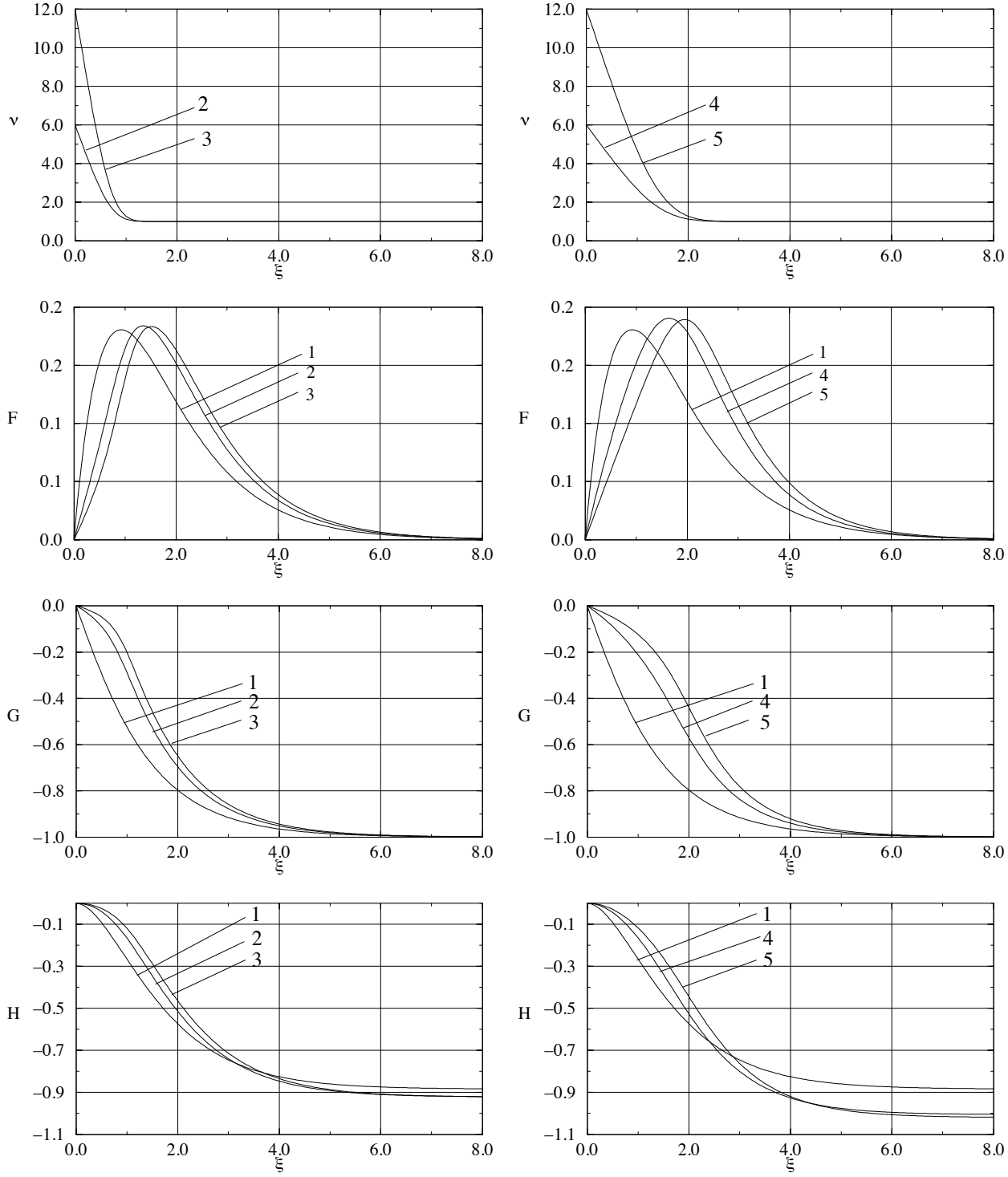

Fig. 2: Dimensionless viscosity, ν, and velocity profiles F, G and H. Curves No. 1 refer to constant viscosity fluids. Curves No. 2: variable viscosity fluids with $q = 15$; Curves No. 3: $q = 2.0$; Curves No. 4: $q = 0.25$ (see Eq. 12).

$$2F + H' = 0 \tag{8}$$

$$F^2 - (G+1)^2 + HF' = \frac{\partial}{\partial \xi}\left(\frac{\nu(\xi)}{\nu(\infty)}F'\right) \tag{9}$$

$$2F(G+1) + HG' = \frac{\partial}{\partial \xi}\left(\frac{\nu(\xi)}{\nu(\infty)}G'\right) \tag{10}$$

$$P' + HH' = 2\frac{\nu'(\xi)}{\nu(\infty)}H' + \frac{\nu(\xi)}{\nu(\infty)}H'' \tag{11}$$

Boundary conditions for F, G and H are $F = H = P = G = 0$ when $\xi = 0$, $F = H' = 0$, $G = -1$ when $\xi \longrightarrow \infty$. In order to integrate Eqs. (8–11) a viscosity profile must be assumed. In this work we use the following profile proposed by Barcia *et. al* (1992):

$$\frac{\nu(\xi)}{\nu(\infty)} = \frac{\nu(0)}{\nu(\infty)} + \left(1 - \frac{\nu(0)}{\nu(\infty)}\right)\frac{q^{1/3}}{\Gamma(4/3)}\int_0^{\xi} e^{-q\xi^3}d\xi \tag{12}$$

The parameter q defines the slope of the viscosity profile close to the electrode surface. Fig. 1 shows the rotating disk used in the experiments conducted by our group. This electrode consists of a $5\,mm$ diameter iron rod embedded in a $10\,mm$ diameter epoxy resin mold such that only its bottom cross section is allowed to contact the electrolyte. Figure 2 shows the non-dimensional viscosity and velocity profiles obtained by numerical integration of Eqs. (8–11) and used in the stability analysis presented in this work. Viscosity profiles with $q = 2.0$ result in a rapid decay of the viscosity to the bulk value, not changing too much the velocity profiles F, G and H. The axial component of the velocity far from the electrode is practically the same of the case with constant viscosity and so is the incoming mass flow approaching the electrode. A decrease in the slope of the viscosity profiles obtained with $q = 0.25$ increases the deviation of the velocity profiles from the constant viscosity case and affects the incoming mass flow rate approaching the electrode.

3. Perturbations of the Base State

We turn now to the question of the stability of the steady configurations of the hydrodynamic field described in Sec. (2), with respect to infinitesimally small disturbances. Variables in Eqs. (1–2) are made non-dimensional as follows: radial and axial coordinates are divided the reference length $(\nu(\infty)/\Omega)^{1/2}$, velocity components are divided by the reference velocity $r_e^*\Omega$, pressure is divided by the reference pressure $\rho r_e^{*}\Omega^2$, viscosity is divided by the bulk value, $\nu^*(\infty)$ and time and the eigenvalue of the linearized problem are made non-dimensional using the factor $\nu(\infty)^{1/2}/(r_e^*\Omega^{3/2})$. Here, r_e^* is the dimensional coordinate along the radial direction where the stability analysis is made. We define also the Reynolds number by the relation:

$$R = r_e^*\left(\frac{\Omega}{\nu(\infty)}\right)^{1/2} \tag{13}$$

The perturbed non-dimensional velocity components and pressure are written as:

$$v_r(t,r,\theta,\xi) = \frac{r}{R}F(\xi) + \tilde{v}_r(t,r,\theta,\xi) \tag{14}$$

$$v_\theta(t,r,\theta,\xi) = \frac{r}{R}G(\xi) + \tilde{v}_\theta(t,r,\theta,\xi) \tag{15}$$

$$v_z(t,r,\theta,\xi) = \frac{1}{R}H(\xi) + \tilde{v}_z(t,r,\theta,\xi) \tag{16}$$

$$p(t,r,\theta,\xi) = \frac{1}{R^2}P(\xi) + \tilde{p}(t,r,\theta,\xi) \tag{17}$$

Substituting the perturbed variables given by (14–17) in the non-dimensional continuity and Navier-Stokes equations and dropping nonlinear terms we obtain:

$$\frac{\tilde{v}_r}{r} + \frac{\partial\tilde{v}_r}{\partial r} + \frac{1}{r}\frac{\partial\tilde{v}_\theta}{\partial\theta} + \frac{\partial\tilde{v}_z}{\partial\xi} = 0 \tag{18}$$

$$\frac{\partial\tilde{v}_r}{\partial t} + \frac{r}{R}F\frac{\partial\tilde{v}_r}{\partial r} + \frac{G}{R}\frac{\partial\tilde{v}_r}{\partial\theta} + \frac{H}{R}\frac{\partial\tilde{v}_r}{\partial\xi} + \frac{F}{R}\tilde{v}_r - \frac{2}{R}(G+1)\tilde{v}_\theta + \frac{r}{R}F'\tilde{v}_z = -\frac{\partial\tilde{p}}{\partial r} + \frac{\nu}{R}\left(\frac{\partial^2\tilde{v}_r}{\partial r^2} + \frac{1}{r^2}\frac{\partial^2\tilde{v}_r}{\partial\theta^2} + \frac{\partial^2\tilde{v}_r}{\partial\xi^2} + \frac{1}{r}\frac{\partial\tilde{v}_r}{\partial r} - \frac{2}{r^2}\frac{\partial\tilde{v}_\theta}{\partial\theta} - \frac{\tilde{v}_r}{r^2}\right) + \frac{\nu'}{R}\left(\frac{\partial\tilde{v}_z}{\partial r} + \frac{\partial\tilde{v}_r}{\partial\xi}\right) \tag{19}$$

$$\frac{\partial\tilde{v}_\theta}{\partial t} + \frac{r}{R}F\frac{\partial\tilde{v}_\theta}{\partial r} + \frac{G}{R}\frac{\partial\tilde{v}_\theta}{\partial\theta} + \frac{H}{R}\frac{\partial\tilde{v}_\theta}{\partial\xi} + \frac{F}{R}\tilde{v}_\theta + \frac{2}{R}(G+1)\tilde{v}_r + \frac{r}{R}G'\tilde{v}_z = -\frac{1}{r}\frac{\partial\tilde{p}}{\partial\theta} + \frac{\nu}{R}\left(\frac{\partial^2\tilde{v}_\theta}{\partial r^2} + \frac{1}{r^2}\frac{\partial^2\tilde{v}_\theta}{\partial\theta^2} + \frac{\partial^2\tilde{v}_\theta}{\partial\xi^2} + \frac{1}{r}\frac{\partial\tilde{v}_\theta}{\partial r} + \frac{2}{r^2}\frac{\partial^2\tilde{v}_r}{\partial\theta^2} - \frac{\tilde{v}_\theta}{r^2}\right) + \frac{\nu'}{R}\left(\frac{1}{r}\frac{\partial\tilde{v}_z}{\partial\theta} + \frac{\partial\tilde{v}_\theta}{\partial\xi}\right) \tag{20}$$

$$\frac{\partial\tilde{v}_z}{\partial t} + \frac{r}{R}F\frac{\partial\tilde{v}_z}{\partial r} + \frac{G}{R}\frac{\partial\tilde{v}_z}{\partial\theta} + \frac{H}{R}\frac{\partial\tilde{v}_z}{\partial\xi} + \frac{H}{R}\tilde{v}_z = -\frac{\partial\tilde{p}}{\partial\xi} + \frac{\nu}{R}\left(\frac{\partial^2\tilde{v}_z}{\partial r^2} + \frac{1}{r^2}\frac{\partial^2\tilde{v}_z}{\partial\theta^2} + \frac{\partial^2\tilde{v}_z}{\partial\xi^2} + \frac{1}{r}\frac{\partial\tilde{v}_z}{\partial r}\right) + 2\frac{\nu'}{R}\frac{\partial\tilde{v}_z}{\partial\xi} \tag{21}$$

At this stage we assume that the perturbation variables are separable and look for a solution in the form:

$$\begin{pmatrix} \tilde{v}_r \\ \tilde{v}_\theta \\ \tilde{v}_z \\ \tilde{p} \end{pmatrix} = \begin{pmatrix} f(\xi) \\ g(\xi) \\ h(\xi) \\ \pi(\xi) \end{pmatrix} \exp[i(\alpha r + \beta R\theta - \omega t)] \tag{22}$$

where ω is a complex number, with $\Re(\omega)$ and $\Im(\omega)$ being, respectively, the frequency and the rate of growth of the perturbation. Parameters α and β are the components of the perturbation wave-vector along the radial and azimuthal directions. For a given time, the phase of the perturbation is constant along branches of a logarithm spiral, with the branches curved in the clockwise direction if β is positive and counter-clockwise, if negative. Substitution of the perturbation variables in Eqs. (18–21) leads to:

$$i\left(\alpha - \frac{i}{r}\right) f + i\frac{R}{r}\beta g + h' = 0 \tag{23}$$

$$i\left(\frac{r}{R}\alpha F + \beta G - \omega\right) f + \frac{r}{R}F'h + i\alpha\pi = \frac{1}{R}\left(\nu f'' - \nu\left(\alpha^2 + \frac{R^2}{r^2}\beta^2\right) f - Ff + 2(G+1)g - Hf' + i\alpha\nu' h + \nu' f'\right) + \frac{1}{R^2}\left(i\frac{R}{r}\nu\alpha f - 2\,i\frac{R^2}{r^2}\nu\beta g\right) - \frac{\nu}{Rr^2}f \tag{24}$$

$$i\left(\frac{r}{R}\alpha F + \beta G - \omega\right) g + \frac{r}{R}G'h + i\frac{R}{r}\beta\pi = \frac{1}{R}\left(\nu g'' - \nu\left(\alpha^2 + \frac{R^2}{r^2}\beta^2\right) g - Fg + 2(G+1)f - Hg' + i\frac{R}{r}\beta\nu' h + \nu' g'\right) + \frac{1}{R^2}\left(i\frac{R}{r}\nu\alpha g - 2\,i\frac{R^2}{r^2}\nu\beta f\right) - \frac{\nu}{Rr^2}g \tag{25}$$

$$i\left(\frac{r}{R}\alpha F + \beta G - \omega\right) h + \pi' = \frac{1}{R}\left(\nu h'' - \nu\left(\alpha^2 + \frac{R^2}{r^2}\beta^2\right) h - Hh' - H'h + 2\,\nu' h'\right) + \frac{i}{Rr}\,\nu\alpha h \tag{26}$$

where $\lambda^2 = \alpha^2 + \beta^2$. Equations (23–26) show that perturbation variables are not, strictly speaking, separable. In order to overcome the problem it is necessary to make the *parallel flow* assumption, usually adopted in stability analysis of growing boundary layers, where variations of the Reynolds number in the stream-wise direction are ignored. Adoption of this hypothesis in rotating disk flow (Malik,1981, 1986, Wilkinson and Malik, 1985, Lingwood, 1995) is made by replacing r by R in Eqs. (23-26):

$$i\left(\alpha - \frac{i}{R}\right) f + i\beta g + h' = 0 \tag{27}$$

$$i\left(\alpha F + \beta G - \omega\right) f + F'h + i\alpha\pi = \frac{1}{R}\left(\nu f'' - \nu\lambda^2 f - Ff + 2(G+1)g - Hf' + i\alpha\nu' h + \nu' f'\right) + \frac{1}{R^2}\left(i\nu\alpha f - 2\,i\nu\beta g\right) - \frac{\nu}{R^3}f \tag{28}$$

$$i\left(\alpha F + \beta G - \omega\right) g + G'h + i\beta\pi = \frac{1}{R}\left(\nu g'' - \nu\lambda^2 g - Fg + 2(G+1)f - Hg' + i\beta\nu' h + \nu' g'\right) + \frac{1}{R^2}\left(i\nu\alpha g - 2\,i\nu\beta f\right) - \frac{\nu}{R^3}g \tag{29}$$

$$i\left(\alpha F + \beta G - \omega\right) h + \pi' = \frac{1}{R}\left(\nu h'' - \nu\lambda^2 h - Hh' - H'h + 2\,\nu' h'\right) + \frac{i}{R^2}\,\nu\alpha h \tag{30}$$

Equations 27–30 reduce to Eqs. 2.16–2.19 given by Malik (1986), in the case of constant viscosity fluids ($\nu = 1,\ \nu' = \nu'' = 0$). By eliminating π, neglecting terms of order R^{-2} and defining $D^n = d^n/d\xi^n$, $\bar{\alpha} = \alpha - i/R$, $\bar{\lambda}^2 = \alpha\bar{\alpha} + \beta^2$ and $\eta = \alpha g - \beta f$ we obtain a sixth order system of two coupled equations in the form:

$$\left(i\nu\left(D^2 - \lambda^2\right)\left(D^2 - \bar{\lambda}^2\right) + i\nu' D\left(2D^2 - \lambda^2 - \bar{\lambda}^2\right) + i\nu''\left(D^2 + \bar{\lambda}^2\right) + R\left(\alpha F + \beta G - \omega\right)\left(D^2 - \bar{\lambda}^2\right) - R\left(\bar{\alpha}F'' + \beta G''\right) - iHD\left(D^2 - \bar{\lambda}^2\right) - iH'\left(D^2 - \bar{\lambda}^2\right) - iFD^2\right) h + \left(2\left(G+1\right)D + 2G'\right)\eta = 0 \tag{31}$$

$$\left(2\left(G+1\right)D - iR\left(\alpha G' - \beta F'\right)\right) h + \left(i\nu\left(D^2 - \lambda^2\right) + i\nu' D + R\left(\alpha F + \beta G - \omega\right) - iHD - iF\right)\eta = 0 \tag{32}$$

Equations 31–32 reduce to Eqs. 2.20–2.21 given by Malik (1986), in the case of constant viscosity fluids and are now rewritten in the form:

$$\begin{pmatrix} a_4D^4 + a_3D^3 + a_2D^2 + a_1D + a_0; & b_1D + b_0 \\ c_1D + c_0; & d_2D^2 + d_1D + d_0 \end{pmatrix} \begin{pmatrix} h \\ \eta \end{pmatrix} = \omega \begin{pmatrix} q_2D^2 + q_0; & 0 \\ 0; & s_0 \end{pmatrix} \begin{pmatrix} h \\ \eta \end{pmatrix} \tag{33}$$

with the coefficients given by:

$$
\begin{aligned}
&a_4 = i\nu \qquad a_3 = i(2\nu' - H)\\
&a_2 = i\nu'' - i\nu\left(\lambda^2 + \bar{\lambda}^2\right) + R\left(\alpha F + \beta G\right) - i\left(H' + F\right)\\
&a_1 = -i\nu'\left(\lambda^2 + \bar{\lambda}^2\right) + iH\bar{\lambda}^2\\
&a_0 = i\bar{\lambda}^2\left(\nu'' + \nu\lambda^2\right) - R\left(\alpha F + \beta G\right)\bar{\lambda}^2 - R\left(\bar{\alpha}F'' + \beta G''\right) + iH'\bar{\lambda}^2\\
&b_1 = 2\left(G + 1\right) \qquad b_0 = 2G'\\
&c_1 = 2\left(G + 1\right) \qquad c_0 = -iR\left(\alpha G' - \beta F'\right)\\
&d_2 = i\nu \qquad d_1 = i\left(\nu' - H\right) \qquad d_0 = -i\nu\lambda^2 + R\left(\alpha F + \beta G\right) - iF\\
&q_2 = R \qquad q_0 = -R\bar{\lambda}^2 \qquad s_0 = R
\end{aligned}
$$

Eq. (33) defines a generalized eigenvalue/eigenfunction problem. The eigenfunctions are the normal modes of the model, the imaginary and real parts of each eigenvalue being, respectively, the rate of growth and the angular velocity of the perturbation relative to the angular velocity of the disk. Positive $\Re(\omega)$ mean perturbations turning angular velocity slower than the disk velocity and negative $\Re(\omega)$ mean perturbations turning faster than the disk.

For a given viscosity profile the parameter space of the problem contains *three* variables, the Reynolds number and the perturbation wave-vector components α and β.

Boundary conditions of the problem require non-slip flow and vanishing axial component of the velocity at the electrode surface. These conditions are already fulfilled by the base-state, so the hydrodynamic field cannot be modified by the perturbation at the electrode surface. In consequence we must require $g = h = 0$ in $\xi = 0$. Moreover, we conclude from Eq. (23) that $h' = 0$ at the electrode surface. In $\xi \longrightarrow \infty$ we require that the perturbation vanishes ($g = h = 0$) and that $h' = 0$.

4. Results

The results are presented in the form of neutral stability curves ($\Im(\omega) = 0$) in the $\beta \times R$ and $\alpha \times R$ planes, for specified values of $\Re(\omega) = \omega_p$, the perturbation frequency, shown in Fig. 3, and the approximate coordinates of the minima of the neutral curves, given in Tables 1 and 2.

Building the neutral curves requires finding the set of points $c(s) = (\alpha(s), \beta(s), R(s))$ that satisfy $F\left(c(s)\right) = 0$, where $F : R^3 -> R^2$ is given by $F = (\Im(\omega), \Re(\omega) - \omega_p)^T$. The neutral curves are built using a Predictor-Corrector Continuation method described in E. Allgower, K. Georg (1991). Here, for completeness, we will give a short description of the employed method:

- The perturbation frequency ω_p is specified and an initial point c_0, in the parameters space α, β, R is given. This point is not necessarily on the neutral curve;
- This initial point is corrected using an inexact Newton iteration given by

$$c_i^{n+1} = c_i^n - F'(c_i^0)^+ F(c_i^n) \tag{34}$$

  where $F'(v_0)^+$ is the pseudo-inverse of Moore-Penrose of the Jacobian of F. The Jacobian is computed numerically, using a finite difference approximation.

- To obtain a new point, first a Predictor step is employed, using a first order Euler approximation:

$$c_{i+1}^0 = c_i + h\ t(F'(c_i)) \tag{35}$$

  where h is a suitable step size, and $t(F'(c_i))$ is the tangent vector to curve $c(s)$.

- The value c_{i+1}^0 is corrected in a Corrector step using Eq. (34) iteratively until a satisfactorily converged value is obtained.
- The generalized eigenvalue/eigenfunction problem required to evaluate $F(c(s))$ is solved numerically, using the LAPACK double precision *zgegv* routine for complex generalized non-symmetric eigenproblems.

Validation of the numerical procedure was done by reproducing neutral curves presented by Malik (1986) and in the Fig. 6 of Lingwood's paper (1995). The neutral curve associated to constant viscosity fluids and $\omega_p = 0$, was built assuming a domain with $\xi_{max} = 30$ and a numerical grid with 601 equally spaced points. All other curves were built in domains with length $\xi_{max} = 25$ and grids with 501 points. According to the validation tests we conducted this result is not significantly affected if larger domains are assumed.

$\Re(\omega)$	Mode 1			Mode 2		
	R	α	β	R	α	β
-0.008	283.9	0.37445	0.09077	–	–	–
0.000	286.3	0.38482	0.07753	452.7	0.13501	0.04698
0.008	292.0	0.39526	0.06471	297.5	0.13813	0.03426
0.024	315.0	0.42371	0.04134	169.0	0.14683	0.009081
0.080	876.8	0.36999	-0.05100	74.38	0.19950	0.06220

Table 1: Approximate coordinates of the minima of the neutral curves No.1 (constant viscosity fluids), shown in Fig. 3.

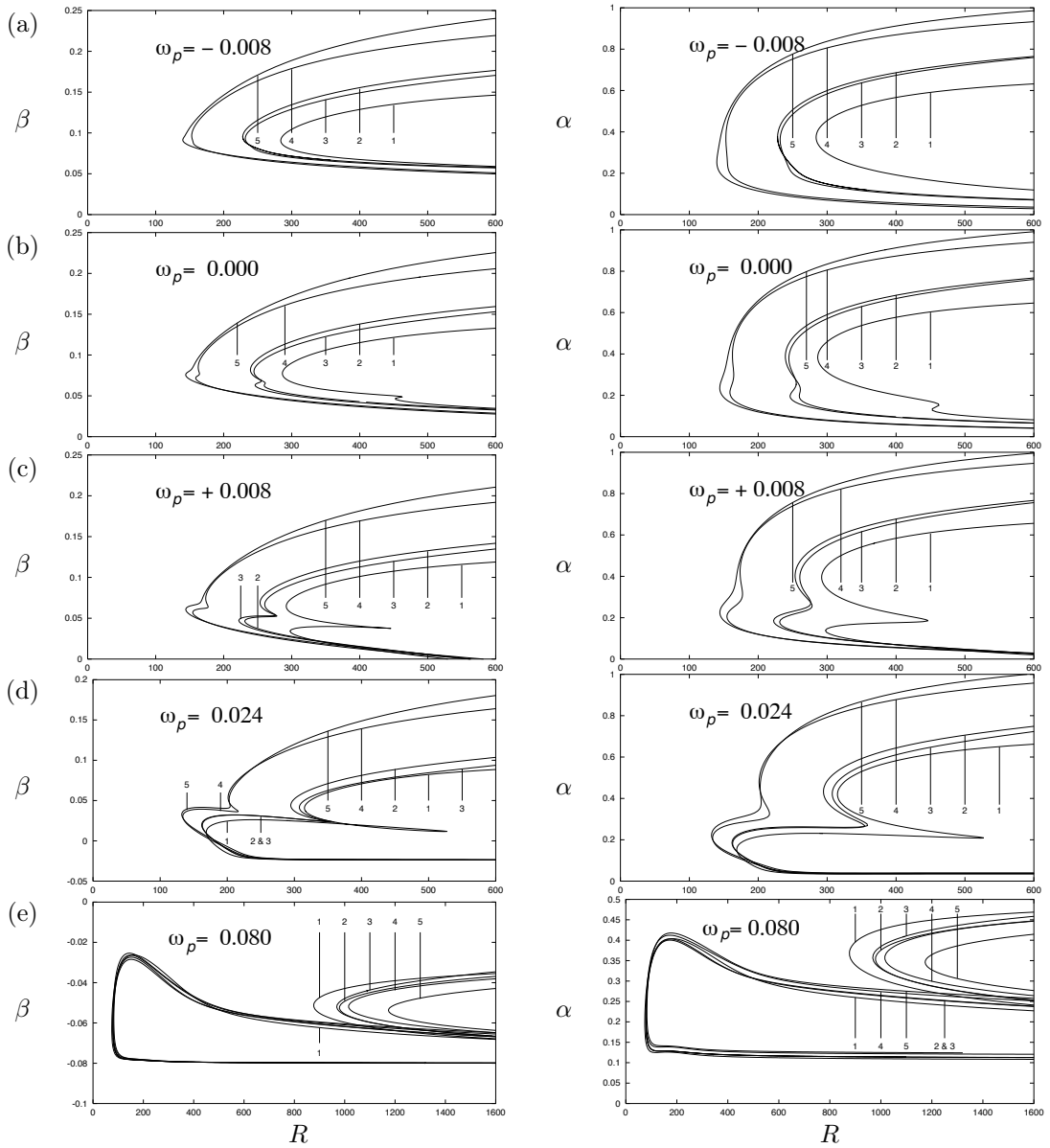

Fig. 3: Neutral curves in the plane $R \times \alpha$ and $R \times \beta$ for $\Re(\omega) = -0.008$ (a), $\Re(\omega) = 0.000$ (b), $\Re(\omega) = 0.008$ (c),$\Re(\omega) = 0.024$ (d) and $\Re(\omega) = 0.080$ (e). Curves No. 1 refer to constant viscosity fluids, the remaining ones, to variable viscosity fluids: Curves No. 2 and 3 refer to fluids with $\nu(0)/\nu(\infty) = 6.0$ and $\nu(0)/\nu(\infty) = 12.0$, respectively, both with $q = 2.00$ (see Eq. 12). Curves No. 4 and 5 refer to fluids with $\nu(0)/\nu(\infty) = 6.0$ and $\nu(0)/\nu(\infty) = 12.0$, respectively, both with $q = 0.25$. In the above diagrams $\omega_p = \Re(\omega)$.

Pontes *et al.* (2002) presented results of neutral stability curves obtained varying α and R for a set of constant β values. Here we present the neutral curves evaluated at the same values of ω_p used by Lingwood (1995) and assuming the four variable viscosity profiles given in section 2. The neutral curves are drawn in the form of stability diagrams plotted in the $R \times \beta$ and $R \times \alpha$ planes, for specified values of $\Re(\omega) = \omega_p$, the perturbation frequency. The angular velocity of the perturbation relative to the disk is given by $\Omega_p = \omega_p/\beta$.

Positive values of Ω_p mean perturbations turning with angular velocity higher than the disk velocity. Malik (1986) studied the case $\Omega_p = 0$, which refers to perturbations turning with the same angular velocity of the disk. Perturbations with negative Ω_p turn slower than the disk.

The neutral curves are shown in Fig. (3) and the main results are briefly summarized below. We begin discussing some general features of the neutral curves, common to both constant and variable viscosity fluids. The first remark is that slower perturbations, with higher values of ω_p, are more unstable, having a lower critical Reynolds numbers than faster perturbations. This effect is well known and this trend remains unchanged when the variable viscosity profile is assumed (Faller, 1991, Lingwood, 1995). Since lower angular velocities Ω_p possibly require the transfer of smaller amounts of energy from the mean flow it seams that this is the reason why slower perturbations tend to have a lower Reynolds number than faster ones.

The second remark refers to the fact that the neutral curves show two branches with the relative position of each one being affected by the frequency ω_p considered. These branches are associated to two different unstable modes, denoted Mode 1 and Mode 2. When $\omega_p = -0.008$ (diagrams *a* in Fig. 3) only the upper branch of the neutral curve for constant viscosity fluids appears in the diagrams, drawn for Reynolds number up to 600. However, the lower branch already appears in diagrams *a* for variable viscosity fluids and the absolute minimum of the neutral curve is located in this branch, for some viscosity profiles considered.

As ω_p increases (diagrams *b* to *e* in Fig. 3) the lower branch moves toward lower Reynolds numbers. In the case of constant viscosity fluids the neutral curve for $\omega_p = 0.008$ (diagram *c* in Fig. 3) displays two minima at the same Reynolds number, approximately. The absolute minimum for variable viscosity fluids is clearly in the lower branch, in these cases. For higher values of ω_p the lower branch moves even more toward lower Reynolds numbers whereas the upper branch moves in the opposite direction. Once more the same trend is observed when a variable viscosity profile is assumed.

Regarding the changes introduced by a variable viscosity profile, we can say that the neutral curves are always affected and, in most cases, in the sense of rendering the flow more *unstable*. However, the effect depends on the perturbation frequency, ω_p, assumed. Figure 3 shows that perturbations with higher frequencies are more affected and reductions in the critical Reynolds number of order of 50% are observed in for $\omega_p = -0.008$, 0 and $+0.008$ (see diagrams *a*, *b* and *c* in Fig. 3). The effect also exists for $\omega_p = -0.024$ but the reduction in the critical Reynolds number is smaller than in the previous cases. And, in case where $\omega_p = 0.080$ variable viscosity renders the flow slightly more stable, with a small increase in minimum of the lower branch (see Fig. 3*e*).

Curves	$\frac{\nu(0)}{\nu(\infty)}$	q	$\Re(\omega)$	Mode 1			Mode 2		
				R	α	β	R	α	β
2	6	2.00	-0.008	228.1	0.37781	0.09585	—	—	—
2	6	2.00	0.000	239.4	0.38577	0.08158	259.6	0.19869	0.06306
2	6	2.00	0.008	253.5	0.40551	0.06925	231.0	0.17967	0.04657
2	6	2.00	0.024	294.7	0.42821	0.04335	162.8	0.18267	0.01949
2	6	2.00	0.080	979.0	0.35147	-0.05283	78.3	0.21117	-0.06048
3	12	2.00	-0.008	233.2	0.32502	0.08928	—	—	—
3	12	2.00	0.000	244.5	0.37891	0.07993	246.2	0.19722	0.06322
3	12	2.00	0.008	260.3	0.39308	0.06666	222.3	0.18654	0.04757
3	12	2.00	0.024	307.4	0.42463	0.04180	161.9	0.18542	0.01968
3	12	2.00	0.080	968.4	0.35644	-0.05217	78.9	0.20667	-0.06155
4	6	0.25	-0.008	153.0	0.36523	0.09634	—	—	—
4	6	0.25	0.000	162.6	0.39755	0.08548	158.9	0.21041	0.07129
4	6	0.25	0.008	173.9	0.39996	0.07168	154.5	0.20400	0.05688
4	6	0.25	0.024	210.2	0.47720	0.05366	133.8	0.20919	0.03038
4	6	0.25	0.080	1015.8	0.35346	-0.05234	79.7	0.22420	-0.05739
5	12	0.25	-0.008	—	—	—	139.9	0.25477	0.09141
5	12	0.25	0.000	—	—	—	144.2	0.23104	0.07533
5	12	0.25	0.008	—	—	—	144.3	0.22959	0.06129
5	12	0.25	0.024	202.9	0.45736	0.05155	132.2	0.22302	0.03277
5	12	0.25	0.080	1173.8	0.34565	-0.05377	82.8	0.22172	-0.05914

Table 2: Approximate coordinates of the minima of the neutral curves No. 2, 3, 4 and 5 (variable viscosity fluids), shown in Fig. 3.

Variable viscosity curves are affected by the $\nu(0)/\nu(\infty)$ ratio and by the parameter q, which defines the thickness of the layer in which the viscosity varies (see Eq. 12 and Fig. 2). The effect of the ratio $\nu(0)/\nu(\infty)$ is, in the range considered in this work, not very important. In general, all curves with $\nu(0)/\nu(\infty) = 12.0$ present the minima at lower Reynolds numbers than curves with $\nu(0)/\nu(\infty) = 6.0$, though the difference is, in most

cases, not large. The exception occurs in the upper branch of the neutral curve for $\omega_p = 0.080$ where, in addition of being more stable than the constant viscosity case, $\nu(0)/\nu(\infty) = 12.0$ is more stable than $\nu(0)/\nu(\infty) = 6.0$.

5. Conclusions

In conclusion we studied the stability of rotating disk flows in electrochemical cells, where the fluid viscosity varies along the axis of the rotating electrode and presented the linear equations governing the evolution of spiral perturbations imposed to the steady flow. These equations reduce to those presented by Malik (1986) in the case of constant viscosity fluids. Comparison of our results for constant viscosity flows, concerning the coordinates of the minimum of the neutral curve for stationary disturbances with results existing in the literature indicate good agreement and provide validation of our numerical code.

Variable viscosity neutral curves, drawn for fixed values of parameter ω_p, indicate that axial viscosity profiles significantly affect the neutral stability curves. Neutral curves associated to a wide range of values of β become more unstable if variable viscosity is assumed. It is interesting to remark that in these cases the flow becomes less stable with an increase in the fluid viscosity close to the disk surface. This decrease of stability is possibly due to the changes introduced in the base state by the viscosity profile.

The results presented support the hypothesis that the current oscillations observed in the polarization curve may originate from a hydrodynamic instability, since the neutral curves presented in this work for variable viscosity fluids show that the critical Reynolds number can be reduced to less than 50% of the value obtained for constant viscosity fluids.

6. Acknowledgments

The numerical calculations were done at the High-Performance Computer Center (NACAD-UFRJ), in the workstations of the Metallurgy and Materials Eng. Dept. (UFRJ) and of the Institute of Mathematics and Computer Sciences (USP-S.Carlos). The authors acknowledge prof. Antônio Castelo Filho (USP-S.Carlos), who developed the numerical code using the Continuation Method to evaluate the neutral stability curves presented in this work. Fruitful discussions with profs. R. E. Kelly from the University of California at Los Angeles and D. Walgraef from the Free University of Brussels are also acknowledged. J. P. received financial support from FAPERJ (Brazil) under the contract number E-26/171.300/2001.

7. References

Allgower, E. and Georg, K., 1991, "Continuation Methods - An Introduction", Springer - Verlag.

Anderson, E., Bai, Z., Bischof, C., Demmel, J., Dongorra, J., Croz, J. D., Greenbaum, A., Hammarling, S., McKenney, A., Ostrouchov, S., and Sorensen, D., 1995, "LAPACK User's Guide", SIAM, Philadelphia, USA.

Barcia, O. E., Mattos, O. R., and Tribollet, B., 1992, Anodic dissolution of iron in acid sulfate under mass transport control, "J. Eletrochem. Soc.", Vol. 139, pp. 446–453.

Epelboin, I., Gabrielli, G., Keddam, M., Lestrach, J. C., and Takenouti, H., 1979, Passivation of Iron in Sulfuric acid Medium, "J. Eletrochem. Soc.", Vol. 126, pp. 1632–1637.

Faller, A. J., 1991, Instability and Transition of the Disturbed Flow Over a Rotating Disk, "J. Fluid Mech.", Vol. 230, pp. 245–269.

Ferreira, J. R. R. M., Barcia, O. E., and Tribollet, B., 1994, Iron dissolution under mass transport control: the effect of viscosity on the current oscillation, "Eletrochim. Acta", Vol. 39, pp. 933–938.

Lingwood, R. J., 1995, Absolute instability of the boundary layer on a rotating disk, "J. Fluid Mech.", Vol. 299, pp. 17–33.

Malik, M. R., 1986, The Neutral Curve for Stationary Disturbances in Rotating-disk Flow, "J. Fluid Mech.", Vol. 164, pp. 275–287.

Malik, M. R., Wilkinson, and Orzag, S. A., 1981, Instability and Transition in a Rotating Disk, "AIAA J.", Vol. 19-9, pp. 1131–1138.

Pontes, J., Conceição, A. R., Mangiavacchi, N., Barcia, O. E., Mattos, O. R., and Tribollet, B., 2002a, Hydrodynamic Stability in an Electrochemical Cell with Rotating Disk Electrode, "Proceedings of the 9^{th} Brazilian Congress of Thermal Engineering and Sciences", Brazil. paper CIT02-0125 (in CD).

Pontes, J., Mangiavacchi, N., Conceição, A. R., Barcia, O. E., Mattos, O. R., and Tribollet, B., 2002b, Instabilities in Electrtochemical Systems with a Rotatinng Disk electrode, "J. of the Braz. Soc. of Mechanical Sciences", Vol. XXIV, pp. 139–148.

Schlichting, H., 1968, "Boundary Layer Theory", McGraw-Hill.

von Kármán, T. and Angew, Z., 1921, Uber Laminare und Turbulente Reibung, "Math. Mec.", Vol. 1, pp. 233–252.

Wilkinson, s. and R., M. M., 1985, Stability Experiments in the Flow Over a Rotating Disk, "AIAA J.", Vol. 23, pp. 588.